

# Anthropogenic activity and climate change exacerbate the spread of pathogenic bacteria in the environment

Yu Geng<sup>1</sup>, Ya Liu<sup>2,3\*</sup>, Peng Li<sup>1</sup>, Jingyu Sun<sup>1</sup>, Yiru Jiang<sup>1</sup>, Zhuo Pan<sup>1</sup>, Yue-Zhong Li<sup>1</sup>, Zheng Zhang<sup>1\*</sup>

Climate change is profoundly affecting human health. Human pathogenic bacteria (HPB) infections mediated by the environment are considered a substantial cause of global health losses. However, the biogeography of HPB and their response to climate change remain largely unknown. Here, we constructed and analyzed a global atlas of potential HPB using 1,066,584 samples worldwide. HPB are widely present in the global environment, and their distribution follows a latitudinal diversity gradient. Climate and anthropogenic factors are identified as major drivers of the global distribution of HPB. Our predictions indicated that by the end of this century, the richness, abundance, and invasion risk of HPB will increase globally, with this upward trend becoming more pronounced as development sustainability declines. Therefore, the threat of environmentally mediated HPB infections to human health may be more severe in a world where anthropogenic activities are intensifying and the global climate is warming.

## INTRODUCTION

Climate change may be the greatest health threat of the 21st century, affecting lives both directly and indirectly through the disruption of environmental and social determinants of health (1–4). Meta-analyses have indicated that human infectious diseases caused by pathogenic microorganisms are exacerbated by climate change (5–7). One of the most critical issues we need to consider is how climate change alters and intensifies the spread of pathogenic bacteria, parasites, fungi, and viruses (8).

Changes in climate and land use will cause species to aggregate in new combinations, facilitating cross-species transmission of viruses (9). Increased heat tolerance in fungi with pathogenic potential due to global warming could lead to new fungal diseases (10). Compared with nonbacterial etiologies, such as fungal infections, malaria, and HIV, infections caused by human pathogenic bacteria (HPB) are the second leading cause of death globally. Annually, bacterial infections contribute to an estimated 7.7 million deaths worldwide (11, 12). Specifically, environmentally mediated transmission is common among human pathogens, and contact with pathogens through water, food, waste, animals, or insect vectors contributes to a major burden of human disease (13). The concept of “One Health” emphasizes that the health of humans, domestic and wild animals, plants, and the wider environment (including ecosystems) are closely linked (14). Despite recent individual studies highlighting pathogen contamination and health risks in environments such as soil (15, 16), wastewater (17), groundwater (18), and ocean (19), there remains a lack of systematic analysis on the distribution characteristics and drivers of HPB in global ecosystems, and the potential impact of climate change on HPB has not been quantified.

Environmental DNA technology allows for the direct extraction of DNA from the environment without relying on pathogen isolation and microscopy, substantially facilitating research on environmental HPB (20, 21). The genetic information of bacteria

obtained by 16S ribosomal RNA (rRNA) amplicon sequencing could be compared with human pathogen databases to reveal the composition, abundance, and distribution of potential HPB in the environment (22). The rapid accumulation of global catalogues of HPB and the extensive sequencing of microbial communities have made it possible to interpret the global distribution and potential health risks of HPB through big data analysis (23). Here, we conducted detection for HPB in more than one million microbial communities across global ecosystems. Through a series of theoretical and modeling methods, we (i) determined the taxonomic composition and distribution of potential HPB in the environment, (ii) mapped their global distribution and revealed the drivers of the richness and abundance of HPB, and (iii) predicted changes in HPB richness and invasion risk under future climate change scenarios.

## RESULTS

### The natural environment has emerged as a reservoir for HPB

We conducted detection for HPB in 1,066,584 sequenced microbial communities, sourced from habitats including animal, plant, soil, and aquatic globally, excluding human-associated habitats (fig. S1). HPB were identified in up to 88% of these natural communities. The detected HPB belonged to 9 phyla, 16 classes, 36 orders, 69 families, 113 genera, and 330 species (table S1). Nearly 90% of these species were predominantly found in the phyla Pseudomonadota, Bacillota, Actinomycetota, and Bacteroidota (Fig. 1A). HPB in natural communities exhibited a latitudinal diversity gradient, with both their richness (Pearson's  $r = -0.15$ ,  $P < 0.0001$ ) and relative abundance (Pearson's  $r = -0.14$ ,  $P < 0.0001$ ) showing weak yet significant negative correlations with absolute latitude (Fig. 1, B and C). On a continental scale, the detection rate (96%), richness (determined on the basis of the operational taxonomic unit (OTU) number of HPB in the microbial communities, median: 9), and relative abundance [parts per million (ppm), median: 3046.0] of HPB in natural communities were highest in Africa, followed by Asia (detection rate: 92%; richness: 9; relative abundance: 1273.0), whereas Antarctica exhibited the lowest values (detection rate: 69%; richness: 2; relative abundance: 53.7) (Fig. 1, D to F).

Copyright © 2025 The Authors, some rights reserved; exclusive licensee American Association for the Advancement of Science. No claim to original U.S. Government Works. Distributed under a Creative Commons Attribution NonCommercial License 4.0 (CC BY-NC).

<sup>1</sup>State Key Laboratory of Microbial Technology, Institute of Microbial Technology, Shandong University, Qingdao 266237, China. <sup>2</sup>Qilu Hospital (Qingdao), Cheeloo College of Medicine, Shandong University, Qingdao 266035, China. <sup>3</sup>Suzhou Research Institute, Shandong University, Suzhou 215123, China.

\*Corresponding author. Email: liuya@sdu.edu.cn (Y.L.); zhangzheng@sdu.edu.cn (Z.Z.)

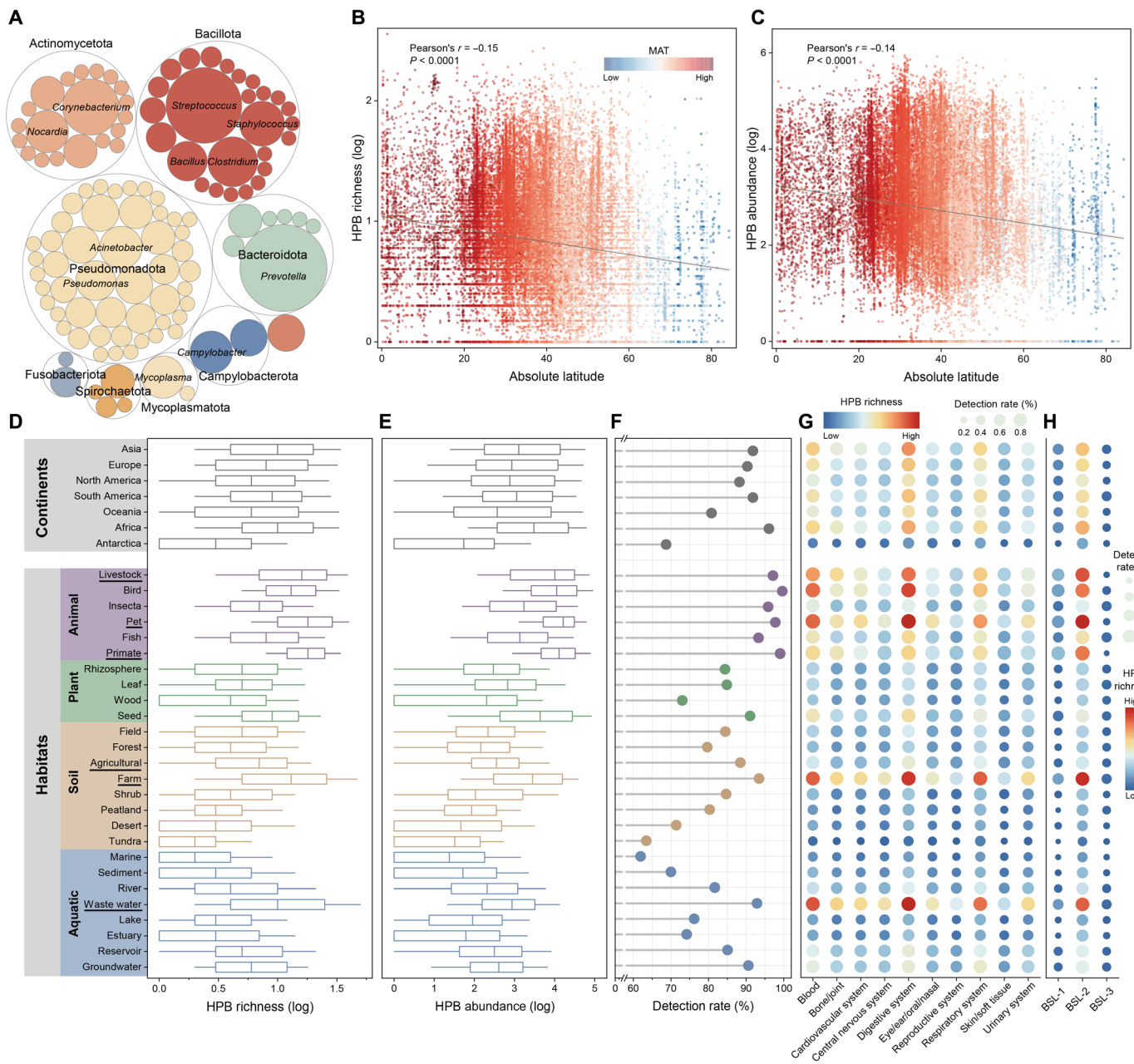


**Fig. 1. Composition and distribution of HPB.** (A) Taxonomy of HPB. The outer and inner circles represent the phyla and genera of HPB, respectively. The circle size is proportional to the number of species. (B and C) Latitudinal distributions of the richness (B) and relative abundance (C) of HPB. In all the depicted scatterplots, the lines indicate the best linear fit, and the shaded areas represent the 95% confidence intervals of the fitted curves. Pearson's correlation tests were used to examine the correlation between the richness and abundance of HPB and absolute latitude, with  $P$  values indicating statistical significance. The color represents the mean annual temperature at the sampling location. (D and E) Richness (D) and abundance (E) of HPB across continents and habitats. Continents are depicted in gray, animal-associated habitats in purple, plant-associated habitats in green, soil habitats in brown, and aquatic habitats in blue. Anthropogenic habitats are underlined. Each continent contains more than 2500 samples, and each habitat surpasses 3500 samples. In all the depicted boxplots, the middle line indicates the median, the box represents the 25th to 75th percentiles, and the error bar indicates the 10th to 90th percentiles of the observations. The richness and abundance values are log-transformed (base 10). (F) Detection rates of HPB across continents and habitats. The detection rate represents the proportion of samples in which HPB was detected to the total number of samples in each continent or habitat. (G and H) Pathogenicity (G) and biosafety levels (H) of HPB across continents and habitats. There are 10 related diseases and three biosafety levels for HPB. The circle size represents the detection rate of HPB for each pathogenicity or biosafety level in each continent or habitat, and the color indicates the richness of HPB.

In terms of various habitats, the detection rates, richness, and relative abundance of HPB were significantly greater in animal-associated (excluding human-associated) habitats than in plant-associated, soil, and aquatic habitats (Fig. 1, D to F, and fig. S2). Specifically, the detection rates of HPB in six animal-associated habitats were not less than 93%, with higher richness and relative abundance observed in pet and primate habitats and lower values in fish and insecta habitats. Among the four plant-associated habitats, seed exhibited the highest detection rate, richness, and relative abundance of HPB, whereas wood demonstrated the lowest values. Across the eight soil habitats, these three metrics ranked the highest in farm and the lowest in tundra. In eight aquatic habitats, the three values of waste water were the highest, and those of marine were the lowest. In particular, the detection rates, richness, and relative abundance of HPB in anthropogenic habitats, such as pet, livestock, primate, farm, agricultural, and waste water, were significantly higher than those in natural habitats (fig. S2).

On the basis of the potential pathogenicity of HPB, detection rates across different continents ranged from 28% (Antarctica, skin/soft tissue) to 91% (Africa, digestive system), while detection rates in various habitats varied between 23% (tundra, skin/soft tissue) and 97% (bird, digestive system) (Fig. 1G). The richness of HPB, which targets the digestive system, was highest in almost all habitat types, whereas the lowest richness was observed for HPB which targets skin/soft tissue. From the perspective of HPB biosafety, the detection rates for biosafety level 1 (BSL-1) ranged from 16% (tundra) to 88% (primate), those for biosafety level 2 (BSL-2) varied between 46% (tundra) and 98% (primate), and those for biosafety level 3 (BSL-3) ranged from 17% (primate) to 52% (farm) (Fig. 1H). Briefly, HPB are widely present in domestic and wild animals, plants, as well as broader soil and aquatic environments, supporting the concept of One Health, which closely links human health with the natural environment.

### Anthropogenic activities facilitate the transmission of HPB among environments

Pathogenic bacteria are closely associated with humans, and we evaluated the relationships between anthropogenic activities and HPB in the environment using collected indicators (table S2). The richness of HPB in natural communities was significantly negatively correlated with life expectancy at birth in each country (Pearson's  $r = -0.25$ ,  $P = 0.008$ ) (Fig. 2A). Furthermore, the richness (Wilcoxon rank-sum test,  $P = 0.003$ ) and relative abundance (Wilcoxon rank-sum test,  $P = 0.030$ ) of HPB in the natural communities of low- and middle-income countries (LMICs) were significantly greater than those in high-income countries (HICs) (Fig. 2B and fig. S3). Similarly, the richness (Wilcoxon rank-sum test,  $P < 0.001$ ) and relative abundance (Wilcoxon rank-sum test,  $P = 0.002$ ) of HPB in countries with high human development levels were significantly greater than those in countries with medium and low human development levels (Fig. 2C and fig. S3). From a national perspective, the richness of HPB was significantly negatively correlated with Human Development Index (HDI, Pearson's  $r = -0.26$ ,  $P = 0.007$ ) and urban population (Pearson's  $r = -0.22$ ,  $P = 0.015$ ) whereas significantly positively correlated with Global Multidimensional Population Index (MPI, Pearson's  $r = 0.38$ ,  $P = 0.003$ ) and mortality rate per 100,000 by pathogen (Pearson's  $r = 0.28$ ,  $P = 0.002$ ) (Fig. 2, D to G). Consequently, socioeconomic factors such as poverty and low urban population might exacerbate the spread of HPB in the natural environment.

HPB exhibited an uneven distribution within natural environments, comprising a low number of high-abundance abundant taxa (species with a relative sequence abundance  $\geq 0.1\%$  across all samples of a habitat) and a high number of low-abundance rare taxa (species with a relative sequence abundance  $< 0.001\%$  across all samples of a habitat) (fig. S4A). Across various habitats, the proportion of rare taxa in HPB ranged from 70.1% (bird) to 94.2% (tundra), whereas the highest proportion of abundant taxa was only 3.2% (livestock). In 11 of these habitats, there were no HPB classified as abundant taxa. Furthermore, there were significant negative correlations between the richness (Pearson's  $r = -0.86$ ,  $P < 0.0001$ ) and relative abundance (Pearson's  $r = -0.86$ ,  $P < 0.0001$ ) of HPB and the proportion of rare taxa (fig. S4, B and C). Given that HPB in the environment are predominantly rare taxa, enhancing the sequencing depth could boost the detection rate of HPB (fig. S4D).

In sharp contrast to the rarity of relative abundance, HPB were mostly widely distributed globally (fig. S5). A total of 94.2% of the HPB species were shared among habitats, and 31.6% of the HPB species were present in all 26 studied habitats (Fig. 2H). The number of resistant drugs in HPB species was significantly positively correlated with both the average detection rate (Pearson's  $r = 0.27$ ,  $P < 0.0001$ ) and average niche breadth (Pearson's  $r = 0.13$ ,  $P = 0.018$ ) in various habitats (Fig. 2, I and J). Overall, HPB primarily constitute rare taxa, yet they are distributed across different habitats in natural environments.

### Global distribution of HPB

To determine the global patterns of HPB richness and abundance, we selected microbial communities with location and environmental information from global samples, excluding data related to oceans and humans for machine learning. Using sample datasets and global covariates (table S3), we constructed random forest models to predict the global patterns of HPB richness and abundance. To avoid multicollinearity during model construction, we estimated the variance inflation factor (VIF) for the covariates and retained those with a VIF lower than 10. On the basis of 10-fold cross-validation, following feature selection and hyperparameter tuning, we identified the optimal feature set consisting of 37 covariates for model construction (fig. S6 and table S4).

Using random forest models, we predicted the richness of HPB at the global scale and mapped its distribution at a resolution of 0.167° (Fig. 3A). The prediction results indicated that HPB richness varied between 1.85 and 27.75 (mean: 9.10; median: 8.80). From a regional perspective, areas with frequent human activities (parts of East Asia), higher temperatures and radiation (parts of Africa and the Middle East), or greater precipitation (Southeast Asia and Central America) exhibited high HPB richness. HPB richness was particularly high in the Indian subcontinent, where human activities and temperatures are high. Conversely, regions with lower temperatures and precipitation and less anthropogenic activity, such as Siberia, Canada, and the Qinghai-Tibetan Plateau, exhibited lower HPB richness. The hotspots of HPB relative abundance differed from those of richness but exhibited similar latitudinal trends, both showing a decreasing trend from low latitudes to high latitudes (Fig. 3B and fig. S7). In addition, after removing common commensal and opportunistic pathogenic bacteria, such as *Escherichia coli*, *Salmonella enterica*, and *Faecalibacterium prausnitzii*, we found that the global distribution and latitudinal trends of HPB richness and abundance were consistent with those without their removal (fig. S8).

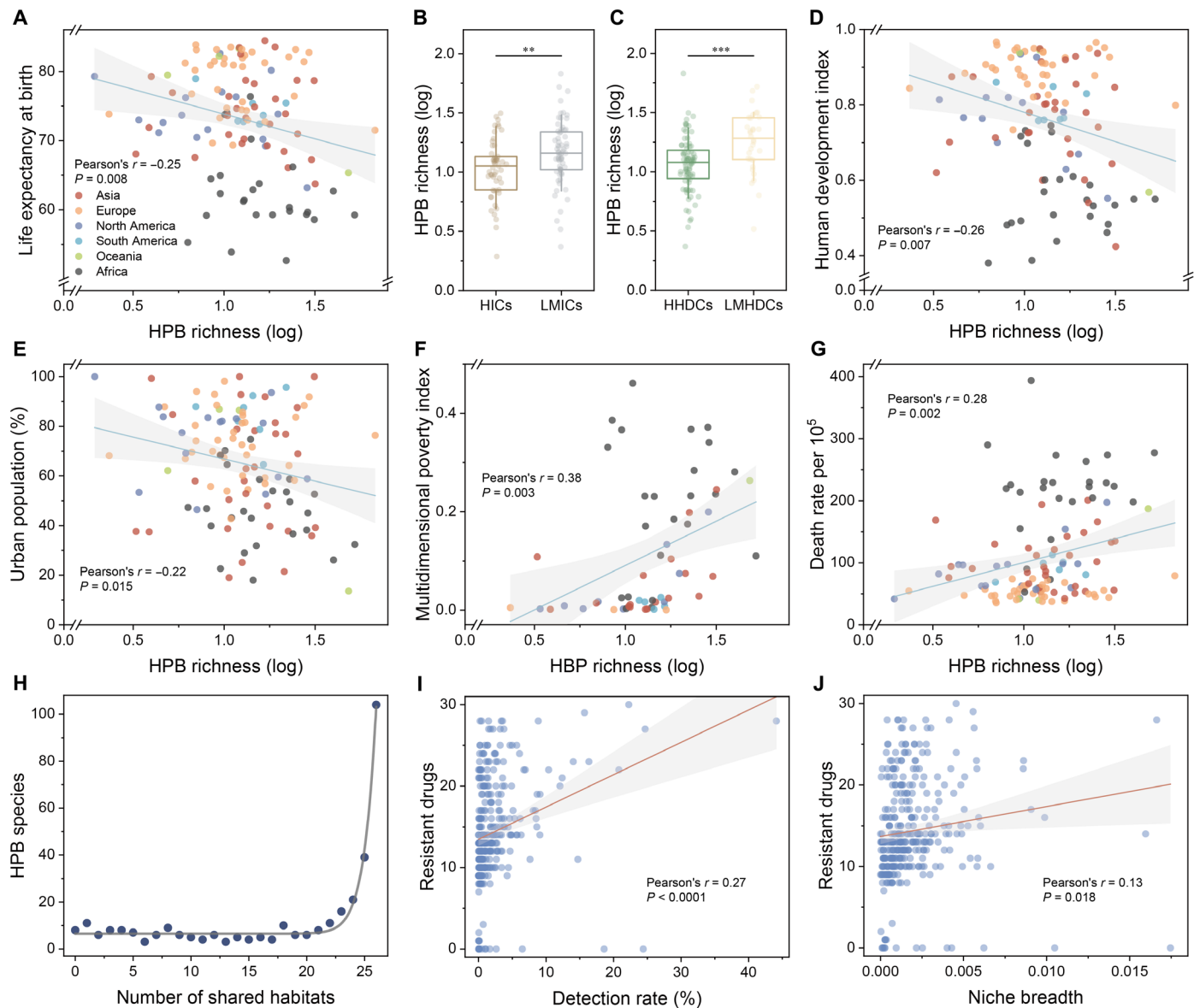


**Fig. 2. Relationships between the richness of HPB and anthropogenic activities.** (A) Relationships between the richness of HPB and life expectancy at birth. Each dot represents a country, and the color indicates the continent where the country is located. Each country contains more than 30 samples. In all the depicted scatterplots, the lines indicate the best linear fit, and the shaded areas represent the 95% confidence intervals of the fitted curves. Pearson's correlation tests were used to examine the correlations, with  $P$  values indicating statistical significance. Richness values are log-transformed (base 10). (B) Differences in the richness of HPB among countries with different income levels. HICs include high income; LMICs include upper middle income, lower middle income, and low income. (C) Differences in the richness of HPB among countries with different levels of human development. High human development countries (HHDCs) include “very high human development” and “high human development”; low and middle human development countries (LMHDCs) include “medium human development” and “low human development.” Comparisons between bins were conducted using the Wilcoxon rank-sum test, \*\* $P < 0.01$  and \*\*\* $P < 0.001$ . In all the depicted boxplots, the middle line indicates the median, the box represents the 25th to 75th percentiles, and the error bar indicates the 10th to 90th percentiles of the observations. (D to G) Relationships between the richness of HPB and socio-economic factors. The socioeconomic factors include HDI (D), urban population (E), Global MPI (F), and mortality rate per 100,000 by pathogen (G). (H) Cross-habitat distribution of HPB. The species was considered to be distributed in the habitat only if it appeared in at least 0.1% of the samples. (I and J) Relationships between the number of resistant drugs and the average detection rate across different habitats (I) or average niche breadth (J).

The global distribution map of HPB suggested that climate factors and anthropogenic activities might have a profound impact on the richness of HPB. We categorized the variables used for model construction into several groups, such as climate factors and anthropogenic factors, and assessed their relative importance in predicting HPB richness (Fig. 3, C and D). The findings emphasized the

significance of climate and anthropogenic activities as primary drivers of HPB richness: climate factors contain the greatest amount of model importance (44.2%), where temperature and precipitation variables each account for nearly 12%, and radiation and moisture variables each contribute more than 5%. Moreover, anthropogenic factors account for more than 30% of model importance. This finding

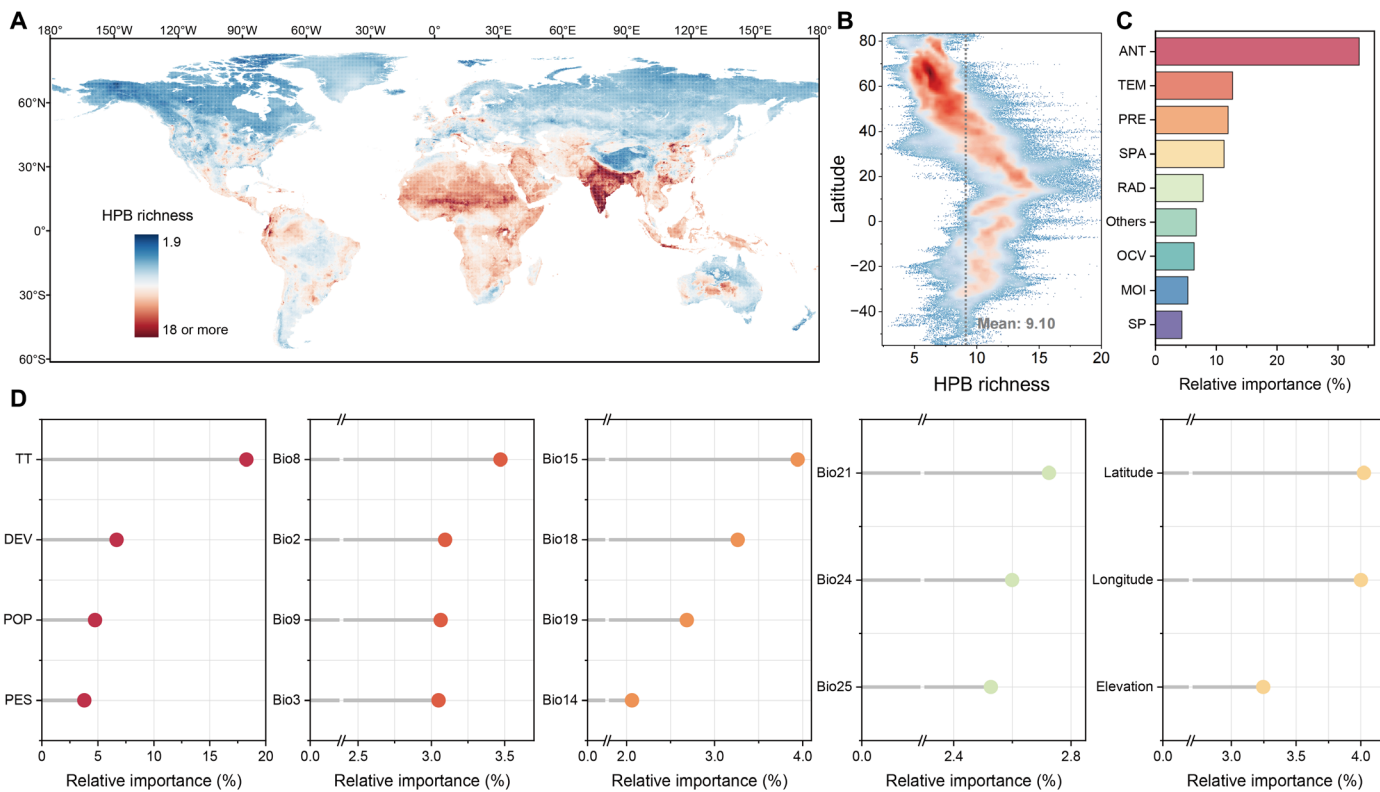


**Fig. 3. Global pattern of HPB richness.** (A) Global map of the richness of HPB. Using covariates, we predicted the richness of HPB globally based on the random forest model. (B) Latitudinal distribution of the global richness of HPB. The dashed line represents the average richness of HPB worldwide. (C) Relative importance of each major category variable in predicting the richness of HPB. ANT, anthropogenic; TEM, temperature; PRE, precipitation; SPA, spatial; RAD, radiation; OCV, other climatic variables; MOI, moisture; SP, soil properties. (D) Relative importance of specific variables of anthropogenic, climate, and spatial factors. From left to right, they represent ANT, TEM, PRE, RAD, and SPA, respectively. TT, travel time; DEV, development; POP, population; PES, pesticide.

indicated that climate and anthropogenic factors, as the two major categories of variables, were responsible for nearly 80% to shaping HPB richness at the spatial scale. Moreover, some spatial variables, such as longitude, latitude, and elevation, also had an impact on the global distribution of HPB richness. Climate has been proven to be a critical factor determining the global distribution of fungi and plant-beneficial bacteria (24–28), and our findings highlighted the importance of climate factors in determining the richness of HPB. In addition, the findings indicated that anthropogenic factors were also the primary factors affecting the global pattern of HPB richness, which could be attributed to human activities promoting the dissemination of HPB across different regions, consequently enhancing their richness.

#### Global richness of HPB under future climate change scenarios

The impact of climate change on the distribution of HPB remains largely uncertain. Therefore, we simulated and predicted the richness of HPB by the end of this century (2081–2100) under four future climate scenarios [shared socioeconomic pathway (SSP) 126, sustainability; SSP245, middle of the road; SSP370, regional rivalry; and SSP585, fossil-fuelled development].

First, we applied multivariate environmental similarity surface (MESS) analysis across the locations of the samples, and the results showed that, except for specific regions such as parts of Antarctica

and the Sahara Desert, the samples used for prediction exhibited high extrapolation reliability for other regions (fig. S9). Through random forest modeling, we projected the global pattern of HPB richness by the end of this century under four scenarios: SSP126, SSP245, SSP370, and SSP585 (Fig. 4A). The findings revealed that HPB richness would increase across all the scenarios, with a greater increase observed as more climate change. Specifically, under the SSP126, SSP245, SSP370, and SSP585 scenarios, HPB richness increased by 11.7, 16.8, 21.5, and 26.6%, respectively (Fig. 4, B and C). This indicated that in scenarios of unsustainable development, the richness of HPB might be promoted. Similarly, a comparable trend was observed in the relative abundance of HPB (fig. S10). Except for certain regions of India, Africa, the Qinghai-Tibetan Plateau, and South America, where HPB richness declined, more than 60% of the areas exhibited upward trends across all the climate scenarios. In terms of latitudinal distribution, with the exception of the Southern Hemisphere mid-latitude region, which experienced more fluctuations, HPB richness was expected to increase in almost all other regions, particularly in the Northern Hemisphere mid-latitude region. After removing common commensal and opportunistic pathogenic bacteria, we evaluated the distribution patterns of remaining HPB richness and abundance under future climate scenarios (fig. S11). The results showed a similar trend of change.

Considering the various continents, HPB richness tended to increase across all continents, with the exception of Antarctica. The

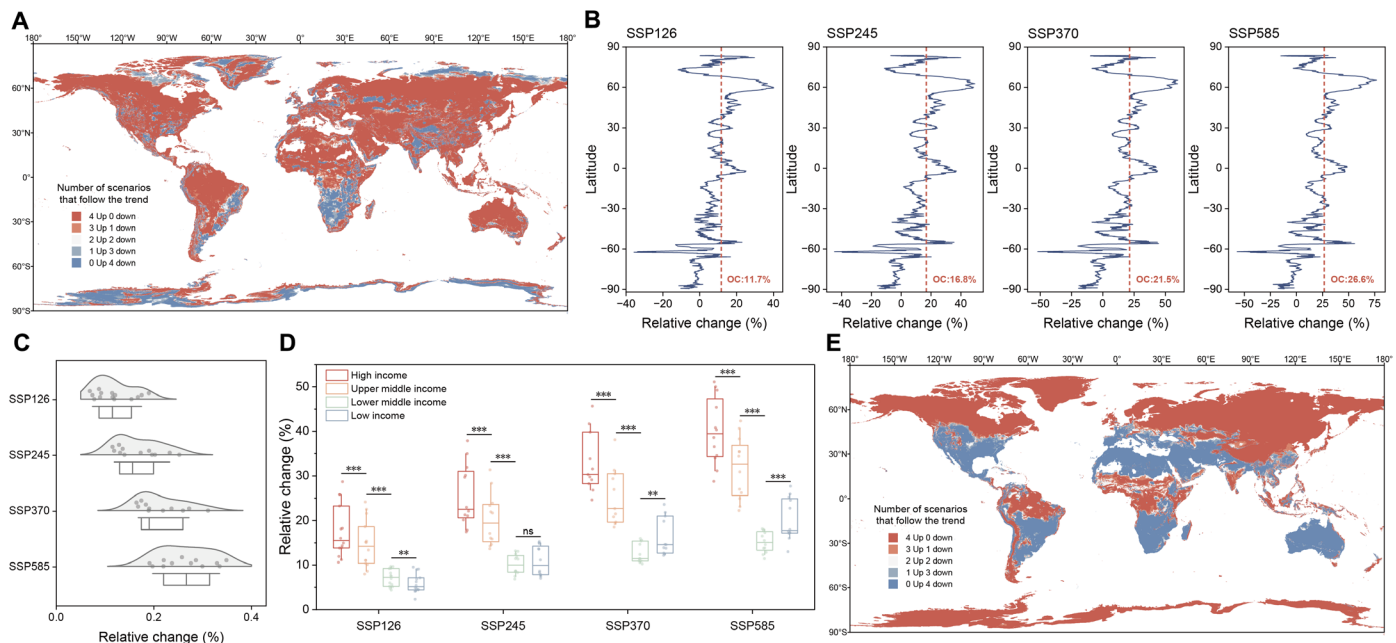


**Fig. 4. Richness and invasion risk of potential HPB under future climate change scenarios.** (A) Relative changes in HPB richness under future climate change scenarios. On the basis of the historical data of 19 bioclimatic variables, a model was constructed using the random forest algorithm to predict the richness of HPB under current climate conditions. Using the constructed model, based on future (2080–2100) data of 19 bioclimatic variables, we predicted future HPB richness under four future climate change scenarios. (B) Latitudinal changes in the richness of HPB under future climate change scenarios. The dashed line represents the overall change (OC) in HPB richness under future climate scenarios compared to the current. SSP126, sustainability; SSP245, middle of the road; SSP370, regional rivalry; SSP585, fossil-fuelled development. (C) Relative changes in the global richness of HPB under future climate change scenarios. (D) Relative changes in the richness of HPB in countries with different income levels under future climate change scenarios. Comparisons between bins were conducted using the Wilcoxon signed-rank test, \*\* $P < 0.01$  and \*\*\* $P < 0.001$ . ns, not significant. In all the depicted boxplots, the middle line indicates the median, the box represents the 25th to 75th percentiles, and the error bar indicates the 10th to 90th percentiles of the observations. Dots represent the changes in richness predicted by different global climate models (GCMs) compared to the current richness. (E) Relative changes in the invasion risk of HPB under future climate change scenarios. “Up” represents the number of scenarios in which HPB richness or invasion risk increases, whereas “down” represents the number of scenarios in which HPB richness or invasion risk decreases under future climate change scenarios.

increase in HPB richness was more pronounced in continents such as Oceania and North America, compared to Africa (fig. S12A). Furthermore, variations in HPB richness were observed across regions with different income levels. The results revealed that the magnitude of the increase in HPB richness was significantly greater in “high income” and “upper middle income” regions than in “lower middle income” and “low income” regions (Fig. 4D). Similarly, the findings related to HDI revealed that the magnitude of the increase in HPB richness in areas with high human development levels was significantly greater than that in areas with medium or low human development levels (fig. S12B). These findings indicated that, compared to those in regions with lower development levels, the magnitude of the increase in HPB richness in regions with higher development levels was more strongly influenced by climate change.

The maximum entropy model has been extensively applied to forecast the species distribution probability of diverse organisms at the global scale (24, 29, 30). Using this model, we evaluated the global invasion risk of HPB under current and different future climate scenarios (Fig. 4E). Under all the climate scenarios, East Asia, Europe, eastern North America, southern South America, and eastern Australia faced high invasion risks, although certain regions within these areas may experience a reduction in invasion risk in the future. Under various climate scenarios, the elevated invasion risks for SSP370 (4.0%) and SSP585 (4.5%) were greater, whereas more sustainable scenarios (SSP126 and SSP245) exhibited increases of

2.6 and 3.2%, respectively (fig. S13). The areas of increased invasion risk were primarily concentrated in the Northern Hemisphere mid-latitude regions. Our findings highlighted the need for sustainable development to limit future HPB invasions, particularly in the Northern Hemisphere mid- and high-latitude regions.

## DISCUSSION

Current infections remain the leading cause of death globally, and the prevalence of pathogenic bacteria in the environment has led to severe human diseases (11, 22). According to the latest list released by the World Health Organization (WHO), the number of pathogens that might trigger the next pandemic has increased to more than 30, including five bacteria (31, 32). To more effectively address public health challenges, the concept of One Health has been proposed, which emphasizes the interdependence of human, animal, plant, and environmental health, aiming to sustainably balance and optimize health (14). Although numerous studies have revealed the intimate connection between specific environments and HPB (15–19), there remains a lack of surveillance of pathogenic bacteria in the environment on a global scale. In this study, we conducted detection for potential HPB in more than one million microbial communities from various habitats including animal, plant, soil, and aquatic globally and ultimately detected HPB in nearly 90% of the communities. The identified HPB were from nine phyla, with 59% of

the species belonging to Pseudomonadota and Bacillota, which contain *E. coli*, *Staphylococcus aureus*, *Streptococcus pneumoniae*, *Klebsiella pneumoniae*, and *Pseudomonas aeruginosa* that are responsible for mass deaths caused by bacteria (11). Focusing on HPB with pandemic potential can help prevent public health emergencies of international concern. Studies have shown that HPB can exploit various habitats and exist in multiple environments, among which environments influenced by human activities are more likely to harbor HPB (33, 34). This observation is consistent with our results, which emphasize that the natural environment can serve as a reservoir for HPB and that environments with closer relationships with humans typically harbor more HPB. We also found that the number of resistant drugs in HPB species was correlated with the detection rate and niche breadth, suggesting that the transmission of HPB between environments may be promoted by antibiotic resistance. These findings support the hypothesis that anthropogenic activities facilitate the transmission of pathogens, reinforcing the concept of One Health (35, 36).

Considerable variation exists in the burden of bacterial infections across different regions, with LMICs bearing the greatest burden of infectious diseases (11, 37, 38). Our results also reflected a correlation between the distribution of HPB and development level. In regions with higher development levels, HPB have lower detection rates, richness, and relative abundance, whereas in regions with lower development levels, these indicators are higher. Regions with higher development levels are associated with more wealth, which can achieve more urban population and improve access to sanitation, clean water, and health care, thereby increasing life expectancy and reducing the mortality rate (13). Socioeconomic drivers play an underappreciated role in the spread of HPB, and poverty and other factors might exacerbate this process. These results support the disease-driven poverty trap hypothesis (39–41), positing that poor people may be ensnared in a reinforced cycle of poverty and disease, in which they are more susceptible to infections mediated by the environment. Our findings highlight the pressing need for better HPB surveillance and control efforts in underdeveloped regions. Although medical advances in the 21st century have promoted progress in human health, inequalities between different countries still exist (42). Therefore, there is an urgent need to increase access to medical services in areas with lower development levels.

In addition to dominant retrospective analysis, more forward-looking research is needed to address potential future changes. Climate change profoundly affects and alters microorganisms on Earth (43–45). Climate extremes disrupt fungal-bacterial interactions, thereby destabilizing soil microbial communities (46). Studies have shown that by the end of this century, fossil fuel-dependent scenarios could lead to a significant decrease of global plant-beneficial bacteria abundance in soils, whereas the diversity and invasive potential of phytopathogenic fungi will increase globally (24, 28). Simultaneously, climate change is having a profound impact on human health, with more than half of human pathogenic diseases being aggravated (5). The profound impact of climate change on HPB has been established: On the one hand, climate change can directly affect specific aspects of pathogens, promoting climate suitability for reproduction, accelerating the life cycle, and increasing virulence (5); on the other hand, climate change indirectly influences pathogens by affecting the reproduction, survival, and geographic distribution of vectors (47). Changes in climate have facilitated cross-species transmission of viruses (9). The adaptation of microorganisms to

higher temperatures may lead to the possibility of previously unrecognized infectious diseases. The increase in heat tolerance of fungi with pathogenic potential, driven by global warming, may lead to the emergence of new fungal diseases (10). Our findings indicated that under future climate scenarios, the richness, relative abundance, and invasion risk of HPB would show upward, with greater increases observed as the sustainability of development decreases. Compared to those in the lower middle income and low income regions, the magnitude of the increase in HPB richness was significantly greater in the high income and upper middle income regions. Although regions with lower levels of development now have higher levels of HPB richness, relative abundance, and bacterial infection burden, climate change also has impact on regions with higher levels of development. To limit the role of climate change in increasing pathogen spillover risk, we must reduce greenhouse gas emissions and pursue sustainable development. In addition, the risk of HPB is shared globally, thus humanity should unite to assist underdeveloped areas in accessing health care and improving medical conditions.

This study provides an omnidirectional understanding on the global biogeography of HPB and the impact of climate change on their distribution. It is important to acknowledge that there remain limitations of our research. This study is based on mapping HPB genome to OTUs, which may mask the complexity in HPB. By attempting to remove common commensal and opportunistic pathogenic bacteria such as *E. coli*, we found that our conclusions remain unchanged. In addition, the  $R^2$  of our machine learning models is less than 0.5, indicating a certain lack of interpretability. However, considering that we used data from more than 10,000 nonredundant locations for machine learning, our models perform robustly. Moreover, the current sample distribution is uneven due to sampling constraints, with sampling points mainly concentrated in the Northern Hemisphere and insufficient sampling in the Southern Hemisphere. Moreover, available data for LMICs remain scarce, despite these countries bearing a greater burden of bacterial infections. Therefore, future efforts should prioritize sampling and research in LMICs. Furthermore, projections for future HPB richness depend on the predominant role of climate covariates in current condition. If there are changes in the key drivers for HPB richness under future climate scenarios, the predictions need to be revised.

In conclusion, we conducted large-scale HPB identification of microbial communities from global ecosystems, identified the taxonomic composition and distribution of potential HPB, and determined their widespread presence in the natural environment. Furthermore, we observed that HPB varied among different habitats and regions with varying development levels, with human activities promoting the dispersal of HPB between environments. Using modeling methods, we created global maps detailing the distribution of HPB richness and relative abundance, assessed the impact of climate change on the distribution of pathogenic bacteria, and found that unsustainable development could exacerbate the dispersal of HPB. The findings indicated the intimate connection between human health and the ecological environment, supporting the concept of One Health. In addition, we found that human activities and climate change could profoundly affect the distribution, richness, and dispersal of HPB in the environment, highlighting the necessity and urgency of reducing greenhouse gas emissions and assisting LMICs in improving medical conditions.

## MATERIALS AND METHODS

### Data collection of HPB

The Global Catalogue of Pathogens (gcPathogen) (23) is a comprehensive genomic resource containing known human pathogens isolated from infected patients, animal hosts, and the environment, aimed at supporting scientific research on pathogens and public health surveillance. Guided by institutions such as the WHO, gcPathogen has compiled a list of human pathogens, including bacteria, fungi, viruses, and parasites. All sequences for the pathogens were obtained from the genomic database of the National Center for Biotechnology Information (NCBI), and the relevant metadata were retrieved from BioSamples and manually curated. This study collected genomic data of HPB from 499 species and extracted information on biosafety levels, number of resistant drugs, and disease for each pathogenic bacterium from the gcPathogen (as of 10 April 2024).

### Data collection of microbial communities

The Microbe Atlas Project (MAP) (48) summarized and organized a large number of sequenced microbial communities, aiming to provide additional perspectives for microbial ecology. The MAP retrieved metadata summary files from the NCBI Sequence Read Archive database and searched for keywords such as “metagenomic,” “microb\*,” “bacteria,” or “archaea.” The raw data were downloaded and quality filtered for all selected sequencing runs. Then, the MAPseq tool was used to assign taxonomic and OTU labels to the filtered reads based on different 16S rRNA gene identity cutoffs (90, 96, 97, 98, and 99%). This study extracted data with OTUs defined at 99% sequence identity, filtered out samples with total rRNA reads less than 10,000 and number of OTUs in the sample less than 20, and removed samples related to humans.

On the basis of the metadata obtained from MAP, we categorized the samples into four major categories of habitats: animal, plant, soil, and aquatic, which were further classified into 26 distinct microbial habitats. Animal-associated habitats were categorized into six types: livestock (including pig, cattle, sheep, and goat), bird (such as sparrow), insecta (such as fruitfly), pet (including cat and dog), fish (such as zebrafish), and primate (such as chimpanzee). Plant-associated habitats were divided into four types: rhizosphere, leaf, wood, and seed. The soil habitats were classified into eight types: field, forest, agricultural, farm, shrub, peatland, desert, and tundra. The aquatic habitats were categorized into eight types: marine (marine, ocean, and sea were all assigned this type), sediment, river, waste water, lake, estuary, reservoir, and groundwater. Anthropogenic habitats represent habitats closely associated with humans, including pet, livestock, primate, farm, agricultural, and waste water.

### Mapping the genomes of HPB to OTUs

We predicted the 16S rRNA gene sequences in HPB genomes collected from the gcPathogen using Barrnap v.0.9 (49) with default parameters. Using the MAPseq v.2.1.1 tool, we mapped the predicted 16S rRNA gene sequences to MAPref v.3.0 (48), which contains 1,360,792 OTU sequences. The outputs provided confidence levels on the mapping between 16S rRNA gene sequences and OTU sequences, and the mapping results that met the following two conditions were chosen: (i) confidence level  $\geq 0.5$ , matching length of 16S rRNA gene sequences and OTU sequences  $\geq 800$ , providing the best match for genomes mapped to multiple OTUs based on the majority principle (proportion  $\geq 50\%$ ); (ii) confidence level  $\geq 0.98$ , matching length between 16S rRNA gene sequences and OTU sequences

$\geq 800$ , providing the best match for genomes mapped to multiple OTUs based on the optimal principle (proportion  $< 50\%$ , but maximum). Moreover, the outputs provided taxonomic labels for each OTU, which we compared with the taxonomic information obtained based on the assembly accession number to remove abnormal results. Ultimately, we identified 733 HPB OTUs within 1,066,584 sequenced microbial communities.

On the basis of the OTU tables retrieved from MAP, we calculated the richness and abundance of pathogenic bacteria in each microbial community, respectively. The richness of HPB was determined on the basis of the OTU number of HPB in the microbial communities, while the abundance of HPB was calculated as follows

$$PA = \text{sum}(OR) / TR \times 10^6$$

where  $PA$  is the abundance of HPB,  $OR$  represents reads of HPB OTUs, and  $TR$  is the total reads of microbial communities.

### Acquisition of socioeconomic factors

We obtained data on HDI and Global MPI from the United Nations (<https://hdr.undp.org/>), with HDI from 2024 and MPI from 2023. Life expectancy at birth, urban population, and income level data were collected from the World Bank (<https://worldbank.org/>), with life expectancy at birth and urban population from 2022 and income level data from the 2024 fiscal year. The mortality rate per 100,000 by pathogen in 2019 was derived from a study conducted in 2022 (11).

### Niche breadth of HPB

Niche breadth is a notable characteristic that affects the relative importance of determinism and stochasticity in community assembly (50), reflecting differences in the adaptability of different species to various environmental conditions. Levins proposed evaluating the niche breadth of species by calculating the evenness of species distribution under various resource states. Levins’ niche breadth index ( $B$ ) was calculated as follows

$$B_j = 1 / \sum_{i=1}^N P_{ij}^2$$

where  $B_j$  represents the niche breadth of species  $j$ ,  $P_{ij}$  represents the proportion of species  $j$  in resource state  $i$ , and  $N$  is the total number of resource states. The range of  $B_j$  is from 1 to  $N$ . Because of different sampling times, the number of resource states also varies, resulting in different ranges of  $B_j$ . For convenience of comparison, it is necessary to standardize  $B_j$  to a range from 0 to 1. Levins’ standardized niche breadth ( $B_A$ ) was calculated as follows

$$B_A = (B - 1) / (N - 1)$$

Last, we calculated the average  $B_A$  of each species ( $B_{avg}$ ) as an indicator of niche breadth.

### Acquisition of gridded covariates

We downloaded historical data for 19 bioclimatic variables from WorldClim, representing the average for the years 1970–2000. Meanwhile, we also extracted future (2080–2100) climate data on these bioclimatic variables. There are four SSPs in future climate data: SSP126: sustainability; SSP245: middle of the road; SSP370: regional rivalry; and SSP585: fossil-fuelled development. Then, we obtained

additional 21 bioclimatic variables from CliMond. Furthermore, we retrieved global maps related to climate variables from other databases. Anthropogenic variables were collected from CGIAR-CSI, DRYAD, and SEDAC, whereas soil properties were derived from SoilGrids. In addition, elevation data were collected from GMTED2010, biomass data were obtained from CDIAC, and plant functional type data were acquired from GCAM. The covariates were categorized into nine types: anthropogenic, temperature, radiation, precipitation, moisture, other climatic variables, soil properties, spatial, and others. Detailed information on the covariates was presented in table S3. To obtain maps of the same resolution, we resampled all the datasets to match the same resolution by using the nearest neighbor method.

### Random forest modeling

First, we processed the data from MAP, selected samples with location information, and excluded data related to oceans and humans. The covariates corresponding to each sampling location were extracted through ArcGIS Pro. Duplicates were removed from samples with the same coordinates, and the richness and abundance of HPB at each location were calculated by averaging. To mitigate spatial autocorrelation, we retained only one sample within 10 m of each other. In addition, we used the blockCV (51) package, which allows for separation of data spatially, ensuring the creation of training and testing sets that are spatially separate.

Then, the global patterns of HPB richness and abundance were estimated using random forest models. First, to avoid multicollinearity, we evaluated the VIF of the variables and removed covariates with a VIF greater than 10. Then, the recursive feature elimination algorithm was used to determine the best combination of features. Afterward, we conducted hyperparameter tuning with the optimal features using grid search to identify the optimal combination of hyperparameters. Both of these procedures were performed on the basis of 10-fold cross-validation, which minimizes the problem of model overfitting. The 10-fold cross-validation  $R^2$  was used to assess the performance of the model. Last, we validated our model on the testing set to evaluate its predictive ability on untrained data (fig. S14).

Last, we set 10 different random seeds to train 10 independent random forest models, calculated the average of 10 predictions as the final results, and calculated the coefficients of variation of the 10 predicted results to evaluate the uncertainty of the model (fig. S14).

The importance of each variable was also determined through machine learning to evaluate the key factors affecting the global distribution of HPB. We estimated the importance of the chosen variables by the function for variable importance measures in the randomForest (52) package of R. For the convenience of comparison, we standardized the importance of these variables on a scale of 0 to 100% to obtain their relative importance (tables S4 and S5).

To verify our results, we used spatial cross-validation with the blockCV package, which offers a range of functions for generating k-fold cross-validation to ensure spatial separation. On the basis of spatial cross-validation, we performed feature selection and hyperparameter tuning to construct models that predict the global patterns of HPB richness and abundance (fig. S15).

### Future richness and abundance projections

A MESS analysis was conducted on the locations of the samples to evaluate the extrapolation reliability of HPB. Using the random forest

algorithm,  $\frac{9}{10}$  of the samples was allocated as the training dataset for the model, whereas  $\frac{1}{10}$  served as the testing set. The dataset used for future projections has also been removed samples with close distances and divided into spatially separate training and testing sets. On the basis of historical data of 19 bioclimatic variables sourced from WorldClim, the global distribution of HPB under the current climate was estimated. The 10-fold cross-validation  $R^2$  was used to assess the performance of the model, and the testing set was used to evaluate its predictive ability on untrained data (fig. S16). Using the established model and based on future (2080–2100) climate data of 19 bioclimatic variables, we predicted the potential richness and abundance of HPB under various future climate scenarios. Each future climate scenario contains multiple different CMIP6 downscaled global climate models (GCMs; table S6), and the projections of different GCMs were averaged. For future projections of HPB richness and abundance, we also used spatial cross-validation to confirm the findings (fig. S17).

### Future invasion risk projection

Using Maxent software, the global invasion risks of HPB under current and future climate conditions were assessed through the maximum entropy model (53). This model has been extensively used for predicting the probability of species distributions of various organisms across the globe. The outcomes represent the predicted probability of suitable conditions, with higher values corresponding to a high likelihood of suitable conditions for HPB and lower values corresponding to a low likelihood. In this study, the prediction probability was considered as invasion risk of HPB. First, the occurrence data of HPB, along with 19 current bioclimatic variables, were imported into Maxent software to generate the global distribution probability of HPB, which reflects the invasion risk. We subsequently projected the future invasion risk of HPB by the end of this century (2081–2100) under four future climate scenarios and assessed the changes in invasion risk relative to the current climate conditions. The following settings were used to run the model: feature classes = auto, replicates = 10, replicated run type = Crossvalidate, maximum iterations = 500, convergence threshold = 0.00001.

### Statistical analyses

The data analysis was mainly conducted using R (version 4.3.3). Through the caret (54) and randomForest (52) packages, the recursive feature elimination algorithm, hyperparameter tuning, and calculation of the relative importance of variables were performed. The partial results were visualized by the ggplot2 (55) package. ArcGIS Pro was used to extract covariates corresponding to location points and visualize the global distribution of HPB.

### Supplementary Materials

#### The PDF file includes:

Figs. S1 to S17

Table S6

Legends for tables S1 to S5

#### Other Supplementary Material for this manuscript includes the following:

Tables S1 to S5

### REFERENCES AND NOTES

1. A. Costello, M. Abbas, A. Allen, S. Ball, S. Bell, R. Bellamy, S. Friel, N. Groce, A. Johnson, M. Kett, Managing the health effects of climate change: Lancet and University College London Institute for Global Health Commission. *Lancet* **373**, 1693–1733 (2009).

2. D. Campbell-Lendrum, T. Neville, C. Schweizer, M. Neira, Climate change and health: Three grand challenges. *Nat. Med.* **29**, 1631–1638 (2023).
3. W. Cai, J. Fanzo, J. Glaser, R. Lowe, A. M. Lusambili, E. Marks, Views on climate change and health. *Nat. Clim. Chang.* **14**, 419–423 (2024).
4. Talking about climate change and health. *Nat. Clim. Chang.* **14**, 409 (2024).
5. C. Mora, T. McKenzie, I. M. Gaw, J. M. Dean, H. von Hammerstein, T. A. Knudson, R. O. Setter, C. Z. Smith, K. M. Webster, J. A. Patz, Over half of known human pathogenic diseases can be aggravated by climate change. *Nat. Clim. Chang.* **12**, 869–875 (2022).
6. M. B. Mahon, A. Sack, O. A. Aleuy, C. Barbera, E. Brown, H. Buelow, D. J. Civitello, J. M. Cohen, L. A. de Wit, M. Forstchen, A meta-analysis on global change drivers and the risk of infectious disease. *Nature* **629**, 830–836 (2024).
7. Climate change exacerbates almost two-thirds of pathogenic diseases affecting humans. *Nat. Clim. Chang.* **12**, 791–792 (2022).
8. Small organisms with big climate impact. *Nat. Microbiol.* **8**, 2213–2214 (2023).
9. C. J. Carlson, G. F. Albery, C. Merow, C. H. Trisos, C. M. Zipfel, E. A. Eskew, K. J. Olival, N. Ross, S. Bansal, Climate change increases cross-species viral transmission risk. *Nature* **607**, 555–562 (2022).
10. A. Casadevall, Global warming could drive the emergence of new fungal pathogens. *Nat. Microbiol.* **8**, 2217–2219 (2023).
11. K. S. Ikuta, L. R. Swetschinski, G. R. Aguilar, F. Sharara, T. Mestrovic, A. P. Gray, N. D. Weaver, E. E. Wool, C. Han, A. G. Hayoon, Global mortality associated with 33 bacterial pathogens in 2019: A systematic analysis for the Global Burden of Disease Study 2019. *Lancet* **400**, 2221–2248 (2022).
12. I. N. Okeke, M. E. A. de Kraker, T. P. Van Boeckel, C. K. Kumar, H. Schmitt, A. C. Gales, S. Bertagnolio, M. Sharland, R. Laxminarayan, The scope of the antimicrobial resistance challenge. *Lancet* **403**, 2426–2438 (2024).
13. S. H. Sokolow, N. Nova, I. J. Jones, C. L. Wood, K. D. Lafferty, A. Gachitorenko, S. R. Hopkins, A. J. Lund, A. J. MacDonald, C. LeBoa, C. LeBoa, A. J. Peel, E. A. Mordecai, M. E. Howard, J. C. Buck, D. Lopez-Carr, M. Barry, M. H. Bonds, G. A. De Leo, Ecological and socioeconomic factors associated with the human burden of environmentally mediated pathogens: A global analysis. *Lancet Planet. Health* **6**, e870–e879 (2022).
14. Tripartite and UNEP support OHHEP's definition of "One Health," WHO (2021).
15. B. K. Singh, Z.-Z. Yan, M. Whittaker, R. Vargas, A. Abdelfattah, Soil microbiomes must be explicitly included in One Health policy. *Nat. Microbiol.* **8**, 1367–1372 (2023).
16. S. Banerjee, M. G. Van Der Heijden, Soil microbiomes and one health. *Nat Rev Microbiol.* **21**, 6–20 (2023).
17. A. G. Shaw, C. Troman, J. O. Akello, K. M. O'Reilly, J. Gauld, S. Grow, N. Grassly, D. Steele, D. Blazes, S. Kumar, The Environmental Surveillance, Defining a research agenda for environmental wastewater surveillance of pathogens. *Nat. Med.* **29**, 2155–2157 (2023).
18. Y. Dong, Z. Jiang, Y. Hu, Y. Jiang, L. Tong, Y. Yu, J. Cheng, Y. He, J. Shi, Y. Wang, Pathogen contamination of groundwater systems and health risks. *Crit. Rev. Environ. Sci. Technol.* **54**, 267–289 (2024).
19. L. Doni, J. Martinez-Urtaza, L. Vezzulli, Searching pathogenic bacteria in the rare biosphere of the ocean. *Curr. Opin. Biotechnol.* **80**, 102894 (2023).
20. K. K. Ko, K. R. Chng, N. Nagarajan, Metagenomics-enabled microbial surveillance. *Nat. Microbiol.* **7**, 486–496 (2022).
21. J. L. Gardy, N. J. Loman, Towards a genomics-informed, real-time, global pathogen surveillance system. *Nat. Rev. Genet.* **19**, 9–20 (2018).
22. D. Zhu, Y. Zhang, Y.-G. Zhu, Human pathogens in the soil ecosystem: Occurrence, dispersal, and study method. *Curr. Opin. Environ. Sci. Health* **33**, 100471 (2023).
23. C. Guo, Q. Chen, G. Fan, Y. Sun, J. Nie, Z. Shen, Z. Meng, Y. Zhou, S. Li, S. Wang, J. Ma, Q. Sun, L. Wu, gcPathogen: A comprehensive genomic resource of human pathogens for public health. *Nucleic Acids Res.* **52**, D714–D723 (2024).
24. P. Li, L. Tedersoo, T. W. Crowther, B. Wang, Y. Shi, L. Kuang, T. Li, M. Wu, M. Liu, L. Luan, Global diversity and biogeography of potential phytopathogenic fungi in a changing world. *Nat. Commun.* **14**, 6482 (2023).
25. L. Tedersoo, M. Bahram, S. Pöhlme, U. Köljalg, N. S. Yorou, R. Wijesundera, L. V. Ruiz, A. M. Vasco-Palacios, P. Q. Thu, A. Suija, Global diversity and geography of soil fungi. *Science* **346**, 1256688 (2014).
26. T. Větrovský, P. Kohout, M. Kopecký, A. Machac, M. Man, B. D. Bahnmann, V. Brabčová, J. Choi, L. Mesárošová, Z. R. Human, C. Lepinay, S. Lladó, R. López-Mondéjar, T. Martinović, T. Mašínová, D. Morais, D. Navrátilová, I. Odriozola, M. Štúrsová, K. Švec, V. Tláskal, M. Urbanová, J. Wan, L. Žifčáková, A. Howe, J. Ladau, K. G. Peay, D. Storch, J. Wild, P. Baldrian, A meta-analysis of global fungal distribution reveals climate-driven patterns. *Nat. Commun.* **10**, 5142 (2019).
27. M. Delgado-Baquerizo, C. A. Guerra, C. Cano-Díaz, E. Egidi, J.-T. Wang, N. Eisenhauer, B. K. Singh, F. T. Maestre, The proportion of soil-borne pathogens increases with warming at the global scale. *Nat. Clim. Change* **10**, 550–554 (2020).
28. P. Li, L. Tedersoo, T. W. Crowther, A. J. Dumbrell, F. Dini-Andreote, M. Bahram, L. Kuang, T. Li, M. Wu, Y. Jiang, L. Luan, M. Saleem, F. T. de Vries, Z. Li, B. Wang, J. Jiang, Fossil-fuel-dependent scenarios could lead to a significant decline of global plant-beneficial bacteria abundance in soils by 2100. *Nat. Food* **4**, 996–1006 (2023).
29. R. Tingley, M. Vallinoto, F. Sequeira, M. R. Kearney, Realized niche shift during a global biological invasion. *Proc. Natl. Acad. Sci. U.S.A.* **111**, 10233–10238 (2014).
30. L. Zhao, J. Li, X. Cui, N. Jia, J. Wei, L. Xia, H. Wang, Y. Zhou, Q. Wang, X. Liu, C. Yin, Y. Pan, H. Wen, Q. Wang, F. Xue, Y. Sun, J. Jiang, S. Li, W. Cao, Distribution of *Haemaphysalis longicornis* and associated pathogens: Analysis of pooled data from a China field survey and global published data. *Lancet Planet Health* **4**, e320–e329 (2020).
31. S. Mallapaty, The pathogens that could spark the next pandemic. *Nature* **632**, 488 (2024).
32. "Pathogens prioritization: A scientific framework for epidemic and pandemic research preparedness," WHO (2024).
33. C. Bonneaud, L. A. Weinert, B. Kuijper, Understanding the emergence of bacterial pathogens in novel hosts. *Philos. Trans. R. Soc. Lond. B Biol. Sci.* **374**, 20180328 (2019).
34. T. Li, K. Feng, S. Wang, X. Yang, X. Peng, Q. Tu, Y. Deng, Beyond water and soil: Air emerges as a major reservoir of human pathogens. *Environ. Int.* **190**, 108869 (2024).
35. R. E. Baker, A. S. Mahmud, I. F. Miller, M. Rajeev, F. Rasambainarivo, B. L. Rice, S. Takahashi, A. J. Tatem, C. E. Wagner, L.-F. Wang, A. Wesolowski, C. J. E. Metcalf, Infectious disease in an era of global change. *Nat. Rev. Microbiol.* **20**, 193–205 (2022).
36. B. A. Jones, D. Grace, R. Kock, S. Alonso, J. Rushton, M. Y. Said, D. McKeever, F. Mutua, J. Young, J. McDermott, D. U. Pfeiffer, Zoonosis emergence linked to agricultural intensification and environmental change. *Proc. Natl. Acad. Sci. U.S.A.* **110**, 8399–8404 (2013).
37. K. E. Rudd, S. C. Johnson, K. M. Agesa, K. A. Shackelford, D. Tsoi, D. R. Kievlan, D. V. Colombara, K. S. Ikuta, N. Kissoon, S. Finfer, C. Fleischmann-Struzek, F. R. Machado, K. K. Reinhart, K. Rowan, C. W. Seymour, R. S. Watson, T. E. West, F. Marinho, S. I. Hay, R. Lozano, A. D. Lopez, D. C. Angus, C. J. L. Murray, M. Naghavi, Global, regional, and national sepsis incidence and mortality, 1990–2017: Analysis for the Global Burden of Disease Study. *Lancet* **395**, 200–211 (2020).
38. A. E. Mather, M. W. Gilmour, S. W. Reid, N. P. French, Foodborne bacterial pathogens: Genome-based approaches for enduring and emerging threats in a complex and changing world. *Nat. Rev. Microbiol.* **22**, 543–555 (2024).
39. M. H. Bonds, A. P. Dobson, D. C. Keenan, Disease ecology, biodiversity, and the latitudinal gradient in income. *PLOS Biol.* **10**, e1001456 (2012).
40. A. Gachitorenko, S. Sokolow, B. Roche, C. Ngonghala, M. Jocque, A. Lund, M. Barry, E. Mordecai, G. Daily, J. Jones, J. R. Andrews, E. Bendavid, S. P. Luby, A. D. La Beaud, K. Seeth, J. F. Guégan, M. H. Bonds, G. A. De Leo, Disease ecology, health and the environment: A framework to account for ecological and socio-economic drivers in the control of neglected tropical diseases. *Philos. Trans. R. Soc. Lond. B Biol. Sci.* **372**, 20160128 (2017).
41. M. H. Bonds, D. C. Keenan, P. Rohani, J. D. Sachs, Poverty trap formed by the ecology of infectious diseases. *Proc. Biol. Sci.* **277**, 1185–1192 (2010).
42. P. J. Hotez, Globalists versus nationalists: Bridging the divide through blue marble health. *PLOS Negl. Trop. Dis.* **13**, e0007156 (2019).
43. European Food Safety Authority, A. Maggiore, A. Afonso, F. Barrucci, G. D. Sanctis, Climate change as a driver of emerging risks for food and feed safety, plant, animal health and nutritional quality. *EFSA Support. Publ.* **17**, 1881E (2020).
44. M. E. Morgado, C. Jiang, J. Zambrana, C. R. Upperman, C. Mitchell, M. Boyle, A. R. Sapkota, A. Sapkota, Climate change, extreme events, and increased risk of salmonellosis: Foodborne diseases active surveillance network (FoodNet), 2004–2014. *Environ. Health* **20**, 105 (2021).
45. R. S. Hellberg, E. Chu, Effects of climate change on the persistence and dispersal of foodborne bacterial pathogens in the outdoor environment: A review. *Crit. Rev. Microbiol.* **42**, 548–572 (2016).
46. J. Shi, M. P. Thakur, Climate extremes disrupt fungal-bacterial interactions. *Nat. Microbiol.* **8**, 2226–2229 (2023).
47. W. M. de Souza, S. C. Weaver, Effects of climate change and human activities on vector-borne diseases. *Nat. Rev. Microbiol.* **22**, 476–491 (2024).
48. J. F. M. Rodrigues, T. S. B. Schmidt, J. Tackmann, C. von Mering, MAPseq: Highly efficient k-mer search with confidence estimates, for rRNA sequence analysis. *Bioinformatics* **33**, 3808–3810 (2017).
49. T. Seemann, barrnap 0.9: Rapid ribosomal RNA prediction. Google Scholar, (2013).
50. W. Wu, H.-P. Lu, A. Sastry, Y.-C. Yeh, G.-C. Gong, W.-C. Chou, C.-H. Hsieh, Contrasting the relative importance of species sorting and dispersal limitation in shaping marine bacterial versus protist communities. *ISME J.* **12**, 485–494 (2018).
51. R. Valavi, J. Elith, J. J. Lahoz-Monfort, G. Guillera-Arroita, blockCV: An r package for generating spatially or environmentally separated folds for k-fold cross-validation of species distribution models. *Methods Ecol. Evol.* **10**, 225–232 (2019).
52. A. Liaw, M. Wiener, Classification and regression by randomForest. *R. News* **2**, 18–22 (2002).
53. S. J. Phillips, M. Dudík, Modeling of species distributions with Maxent: New extensions and a comprehensive evaluation. *Ecography* **31**, 161–175 (2008).
54. M. Kuhn, Building predictive models in R using the caret package. *J. Stat. Softw.* **28**, 1–26 (2008).
55. H. Wickham, *ggplot2: Elegant Graphics for Data Analysis* (Springer-Verlag New York, 2016).

**Acknowledgments**

**Funding:** This work was supported by the Science and Technology Fundamental Resources Investigation Program (2022FY101100 to Z.Z.), the National Natural Science Foundation of China (32270073 to Z.Z. and 32401327 to Y.L.), the Science Foundation for Youths of Shandong Province (ZR2022QC001 to Y.L.), and the Natural Science Foundation of Jiangsu Province (BK20230248 to Y.L.). **Author contributions:** Writing—original draft: Y.G., Z.Z., Y.L., P.L., Y.J., and Y.-Z.L. Conceptualization: Y.G., Z.Z., Y.L., and Y.-Z.L. Investigation: Y.G., Z.Z., and Y.L. Writing—review and editing: Y.G., Z.Z., Y.L., P.L., J.S., Y.J., Z.P., and Y.-Z.L. Methodology: Y.G., Z.Z., and Y.L. Resources: Y.G., Z.Z., and Y.L. Funding acquisition: Z.Z. and Y.L. Data curation: Y.G., Z.Z., Y.L., and J.S. Validation: Y.G., Z.Z., Y.L., P.L., J.S., and Y.J. Supervision: Z.Z. and Y.L. Formal analysis: Y.G., Z.Z., Y.L., P.L., J.S., and Y.J. Software: Y.G., Z.Z., P.L., and J.S. Project administration: Z.Z. and Y.L. Visualization: Y.G., Z.Z., and Y.L. **Competing interests:** The authors declare that they have no competing interests. **Data and materials availability:** All data needed to evaluate the conclusions in the paper are present in the paper and/or the

Supplementary Materials. All genomic data of HPB are available in the gcPathogen database (<https://nmdc.cn/gcpathogen/>). All microbial communities and samples are available in the MAP database (<https://microbeatlabs.org/>). The socioeconomic factors used in the current study are available from the United Nations (<https://hdr.undp.org/>) and the World Bank (<https://worldbank.org/>). The current and future climate data are available from WorldClim (<https://worldclim.org/>). Detailed information on the other covariates used in the current study is presented in table S3. Source data are provided with this paper. All the codes for machine learning and statistical analysis used in this study are available online at <https://doi.org/10.5061/dryad.msbcc2g82>.

Submitted 15 August 2024

Accepted 21 February 2025

Published 26 March 2025

10.1126/sciadv.ads4355